4R.3 IDENTIFICATION AND REMOVAL OF NON-PRECIPITATION ECHOES USING THE CHARACTERISTICS OF RADAR ECHOES

GyuWon Lee*,[1], Yo-Han Cho[2], Kyung-Eak Kim[2], and Isztar Zawadzki[1]

[1]J. S. Marshall Radar Observatory, McGill University, Montreal, Quebec, Canada
[2]Dept. of Astronomy and Atmospheric sciences, KyungPook National University, Taegu, Korea (ROK)

1. INTRODUCTION

The purpose of this paper is to develop a method of detecting non-precipitation echoes (mostly AP or normal ground echoes) based on radar echo characteristics. The membership functions and weights for the fuzzy logic are objectively derived from the statistics of observed echo characteristics (the absolute Doppler radial velocity, the standard deviation of reflectivity, and the vertical gradient of reflectivity) as a function of reflectivity to optimize the removal of non-precipitation echoes.

2. DATA

The characteristics of radar echoes are obtained from five non-precipitation and precipitation events. Over 460 volume scans (~ 40 hours) from McGill S-band operational polarimetric radar are used. The five non-precipitation cases include hours with normal ground echoes as well as with noticeable AP. The five precipitation cases have no AP and include stratiform rain, convective lines, and isolated small convective cells. For the validation of an AP removal algorithm, a different data set is used. This data set includes various meteorological situations to test the applicability of an algorithm (stratiform rain, scattered showers associated with small shallow convective cells, and strong convective lines). In some cases, strong AP occurs simultaneously with precipitation.

3. Methodology

a. Identification of precipitation and non-precipitation echoes

The removal of non-precipitation echoes is performed at a resolution of 1 km and 1 deg.. The algorithm uses three parameters (or features) derived at that resolution: the standard deviation of reflectivity (SDZ in dB), the vertical gradient of reflectivity (VGZ in dB deg.$^{-1}$), and the absolute Doppler radial velocity (V_r in m s^{-1}).

$$SDZ = \left[\frac{1}{n} \sum_{j=1}^{n} \left(dBZ_j - \overline{dBZ} \right)^2 \right]^{1/2}$$

$$VGZ = -\frac{dBZ_{i+2} - dBZ_i}{\theta_{i+2} - \theta_i} \qquad (1)$$

where the indexes i and j are for the elevation angles and ranges, respectively. The *n* is the number of reflectivity measurement within 1-km range. Similar parameters are used in the previous researches by Kessinger et al. (2001) and Steiner and Smith (2002). During data archiving procedure, SDZ is calculated from high-resolution (150 m by 1 deg) raw data. We combine all three parameters with proper weights to compensate for the weakness of each parameter in the context of a fuzzy logic approach. The overall procedure is described in Fig. 1.

The reflectivity value of non-precipitation echoes, that are identified with this procedure, is switched to the reflectivity offset value that is corresponding to no rain. In this paper, we have not applied any interpolation or extrapolation over the non-precipitation echoes because we first want to test the performance of this procedure. Unlike other studies in the literature, the current method is performed for entire set of 24 elevation angles except for last two.

b. Validation methods

We evaluate the performance of the algorithm in two ways: 1) by examining the resultant rainfall accumulation maps and 2) by comparing with polarimetric identification of non-precipitation echoes at all PPIs. The climatological R-Z relationship ($Z = 210R^{1.47}$) in Montreal (Lee and Zawadzki 2005) is used for the transformation of the measured reflectivities.

The polarimetric identification of non-precipitation echoes can be considered as reliable reference for validation (Giuli et al. 1991; Ryzhkov and Zrnic 1998). The polarimetric approach adapted by the operational McGill S-band radar is based on the standard deviations of the differential reflectivity (Z_{DR}), of the phase shift (ϕ_{DP}), and of reflectivity (Z). They are computed over a 1-km range using the measurements obtained at each pulse length of 150 m. The membership functions of our polarimetric approach are almost step functions with thresholds of $SD_{Z_{DR}}$ = 1.6 dB, $SD_{\phi_{DP}}$ = 14 deg., SD_Z = 3.4 dB. The same weight is applied to each parameter. Consequently, when two of these standard deviations are larger than the corresponding threshold values, that is, the total membership value exceeds 0.66, the pixel is considered as a "true" non-precipitation echo. The classification of this approach is taken to be the truth for evaluating the skill of our proposed method outlined in Fig. 1, Four skill scores [the probability of detection (POD), the false-alarm rate (FAR), the critical success index (CSI) and equitable threat score (ETS)] are calculated. In addition to these skill scores, rainfall accumulation maps are compared after eliminating non-precipitation echoes with the proposed and polarimetric methods.

* *Corresponding author address:* GyuWon Lee, J. S. Marshall Radar Observatory, P. O. Box 198, Macdonald Campus, Ste-Anne-de-Bellevue, QC, Canada, H9X 3V9
e-mail: gyuwon.lee@mail.mcgill.ca

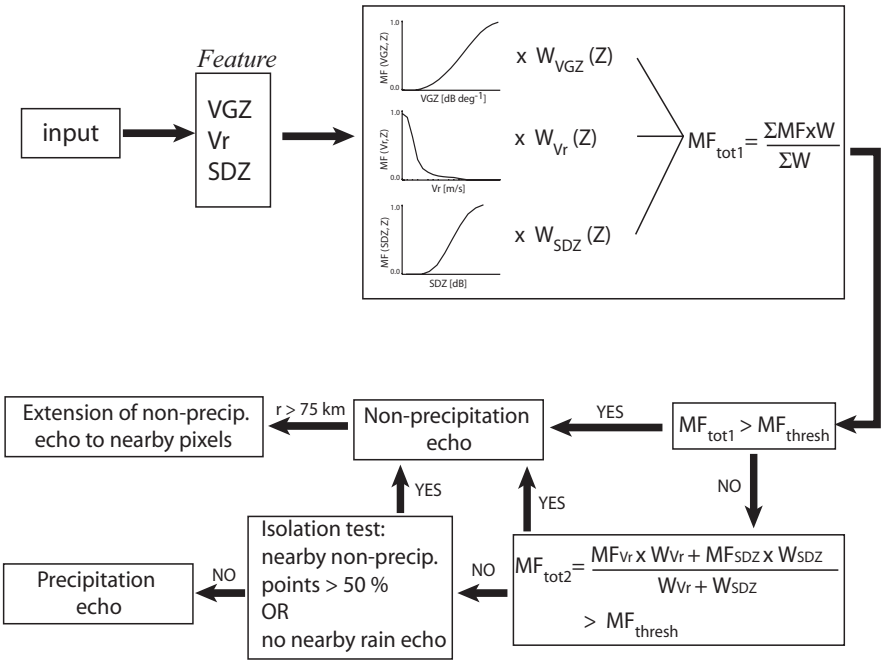

Fig. 1: A schematic diagram for the determination of non-precipitation and precipitation echoes. Three features are calculated: the vertical gradient of reflectivity (VGZ), the absolute Doppler radial velocity (Vr), and the standard deviation of reflectivity (SDZ). The total weighted membership function (MF_{tot1}) is obtained with proper weights (W). This value is then compared with a pre-determined threshold value (MF_{thresh} = 0.55). When $MF_{tot1} > MF_{thresh}$, this point is identified as a non-precipitation echo and the extension of non-precipitation echo to nearby pixels is applied when the range is larger than 75 km. When $MF_{tot1} \leq MF_{thresh}$, this point is further tested with another total membership value (MF_{tot2}) that is derived from only SDZ and Vr. This test required to identify AP under low bright band conditions.

4. Membership functions and their weights

a. Radar echo characteristics

We have derived the normalized frequency distributions of the three parameters (VGZ, Vr, and SDZ) to define the characteristics of normal ground, AP, and precipitation echoes. Similar studies on radar echo characteristics have been conducted by Grecu and Krajewski (2000) and Steiner et al. (1999). Pixels in the three dimensional volume scans where the reflectivity of the average ground echoes (Z_{GRE}) is larger than a radar offset value (Z_{offset}) of about -23 ~ -20 dBZ are labeled as "normal ground echoes (GRE)" for the clear air events. The remaining pixels with echoes exceeding the offset are categorized as Anomalous Precipitation (AP). Precipitation echoes (PRE) are areas of all three dimensional volumes scans for the precipitation events with $Z_{GRE} = Z_{offset}$. The average ground echo map is derived from a data set of clear but no-AP conditions for an entire month. Figs. 2, 3, and 4 show reflectivity dependent distributions of the three parameters for only two categories [non-PRE, that is, GRE+AP, and PRE].

In general, the distributions of the three parameters for PRE do not vary with reflectivity whereas significant variations for non-PRE are noticeable. The PRE distribution of Vr is independent of reflectivity. The one for non-PRE becomes narrower with higher Z, indicating the greater stationarity of strong non-precipitation echoes. The broader Vr distribution at weaker reflectivity is an indication of the contamination by biological insects.

Similarly, the distribution of SDZ for PRE remains unchanged for the different intervals of reflectivity. However, that of non-PRE becomes broader and shifts to larger SDZ value with increasing Z, resulting into a reduction of the overlapping area. This is an indication that SDZ is a better separator of the two classes at higher reflectivity. Thus, higher AP or GRE can be eliminated more effectively than weaker non-precipitation echoes.

The distribution of VGZ for precipitation (PRE) does not vary with reflectivity while that for non-precipitation echoes (non-PRE) changes significantly. However, no separation between distributions for PRE and non-PRE is present at the weakest reflectivity (Z = 0 ~ 10 dBZ), indicating that VGZ at this range of Z cannot be used for identification. The distribution for non-PRE gradually shifts to larger VGZ with increasing Z and shows two distinctive peaks. An examination of the data reveals that the contribution for the first peak is mainly from areas of normal ground echoes whereas the second peak is due mainly to AP. A prominent separation occurs for Z > 30 dBZ. Without further investigation, it is clear that VGZ is the best parameter for higher reflectivity and should thus have the largest weight.

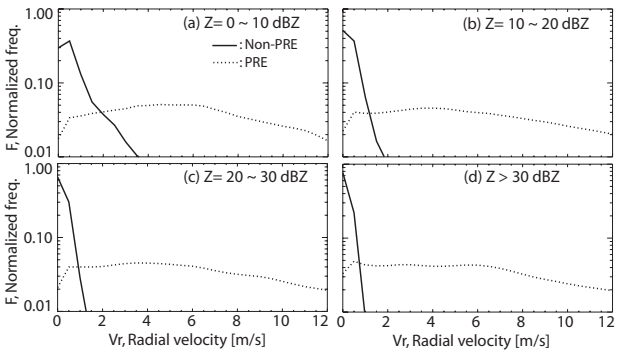

Fig. 2 (Above) Normalized frequency distributions (F) of the absolute Doppler radial velocity (Vr) for non-precipitation (non-PRE) and precipitation (PRE) echoes as a function of reflectivity. The distributions are derived from the entire volume scans of ten events. Near constant distribution for PRE is noticeable. Note that the distributions are shown only for F > 0.01.

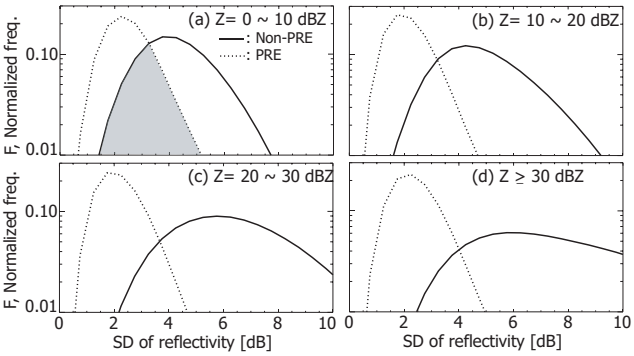

Fig. 3 (Right-above) Same as Fig. 2 except for the standard deviation of reflectivity (SDZ).

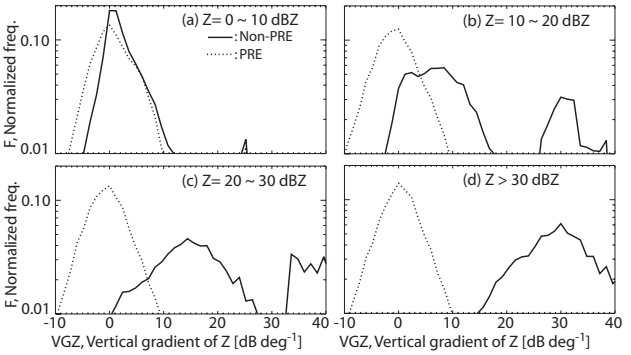

Fig. 4 (Right) Same as Fig. 4 except for the vertical gradient of reflectivity (VGZ).

b. Membership functions

From the characteristics of precipitation and non-precipitation echoes, we now construct membership functions that are used for the identification of non-precipitation echoes. For a given parameter (for an example, SDZ) and reflectivity interval, we have two normalized frequencies for non-precipitation ($F_{non-PRE}$) and for precipitation (F_{PRE}) echoes. The membership function $MF_{non-PRE}(SDZ_i, Z)$ of non-precipitation echoes is derived from the following:

$$MF_{non-PRE}(SDZ_i, Z) = \frac{F_{non-PRE}(SDZ_i, Z)}{F_{PRE}(SDZ_i, Z) + F_{non-PRE}(SDZ_i, Z)} \quad (2)$$

where Z indicates the interval of reflectivity selected for Figs. 2, 3, and 4. In addition, the membership function for the entire range of reflectivity is also derived.

The derived membership functions for the selected reflectivity intervals are shown in Fig. 5. The VGZ membership function for 0 ≤ Z< 10 dBZ is not derived because, as seen in Fig. 4a, the two $F_{non-PRE}$ and F_{PRE} are unable to separate the PRE and non-PRE classes.

It is noticeable that the membership functions do vary as a function of reflectivity intervals. For example, when $SDZ_i = 4\ dB$, $MF_{non-PRE}$ increases from 0.5 when Z ≥ 30 dBZ to 0.8 when 10 ≤ Z < 20 dBZ. $MF_{non-PRE}(Vr_i, Z)$ becomes broader as the reflectivity decreases. The change of $MF_{non-PRE}(VGZ_i, Z)$ is rather dramatic. An echo with $VGZ_i = 10\ dB$ is favorable to be non-precipitation echo when 10 ≤ Z < 20 dBZ ($MF_{no-PRE} = 0.8$) whereas it is more likely to be precipitation when Z ≥ 30 dBZ ($MF_{no-PRE} = 0.3$). This emphasizes the importance of stratifying membership functions with different reflectivity. Traditionally, only one membership function has been used for the entire range of reflectivity (Kessinger et al. 2001). If a membership function for the entire range of Z was used, the 30 dBZ echo would have been incorrectly classified as non-precipitation echo. In general, for a given value of parameters (SDZ, Vr, and VGZ), a single membership function for the entire reflectivity range leads to a mis-identification whereby heavy precipitation is unnecessarily removed and weak non-precipitation echoes remain.

c. Weights of membership functions

The weights can be easily calculated by comparing overlapping areas of each parameter since they represent the ambiguity between non-precipitation and precipitation echoes. For a given reflectivity interval, the weights are calculated from the following:

$$w_{SDZ}(Z) = \frac{1}{A_{SDZ}} \times \frac{1}{S}$$
$$w_{VGZ}(Z) = \frac{1}{A_{VGZ}} \times \frac{1}{S} \quad (3)$$
$$w_{Vr}(Z) = \frac{1}{A_{Vr}} \times \frac{1}{S}$$

where $S = 1/A_{SDZ} + 1/A_{VGZ} + 1/A_{Vr}$ and *A* is the overlapping area between normalized frequencies of non-precipitation and of precipitation echoes (shaded area in Fig.3a as an example). The calculated weights

and overlapping areas are listed in Table 1. Considering the entire range of reflectivity, the Vr is the most important parameter and followed by VGZ. As reflectivity increases, the VGZ becomes more dominant while the opposite occurs for Vr. The changing weights with reflectivity underline the necessity of classifying the membership functions according to reflectivity. The increase of the total overlapping area (the last column in Table 1) with decreasing reflectivity indicates the greater ambiguity in separating non-precipitation echoes from precipitation, in other words, stronger non-precipitation echoes are easier to identify than weaker echoes.

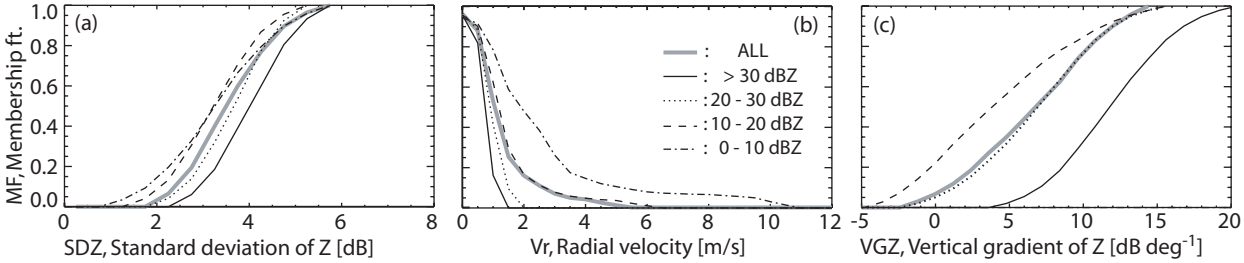

Fig. 5: Membership functions for three parameters that are derived from the characteristics of radar echoes in Figs. 2, 3, and 4. Different lines indicate different intervals of reflectivity.

Table 1: Weights (w) of membership functions and overlapping areas (A) between normalized frequencies for precipitation and non-precipitation echoes for different reflectivity intervals.

Reflectivity intervals	Vertical gradient of reflectivity (VGZ)		Standard deviation of reflectivity (SDZ)		Absolute Doppler radial velocity (Vr)		Total area
	Area (A)	Weight (w)	A	w	A	w	
Z ≥ 30 dBZ	0.055	0.512	0.159	0.178	0.092	0.309	0.306
20 ≤ Z < 30	0.170	0.269	0.165	0.277	0.101	0.454	0.437
10 ≤ Z < 20	0.388	0.205	0.282	0.282	0.156	0.512	0.826
0 ≤ Z < 10	-	-	0.438	0.384	0.273	0.616	0.711
ALL	0.155	0.301	0.169	0.276	0.11	0.424	0.434

5. Evaluation

a. Two tests: MF_{tot1} and MF_{tot2}.

VGZ for non-precipitation echoes can be small under bright band conditions, identifying them as precipitation echoes. Thus, in order to minimize the effects of a bright band, we apply an additional test with MF_{tot2} that is a weighted sum of the membership values of SDZ and Vr. Skill scores after identifying non-precipitation with $MF_{tot1} > MF_{thresh}$ and $MF_{tot2} > MF_{thresh}$ is shown in Fig. 6 for the case of 8 July 2004. POD, CSI, and ETS at $MF_{thresh} > 0.6$ are significantly improved with $MF_{tot2} > MF_{thresh}$ although FAR is slightly worse. Lower skill scores (not shown here) would be achieved by applying only MF_{tot2}. The additional test of $MF_{tot2} > MF_{thresh}$, slightly improves POD, CSI, and ETS scores at $MF_{thresh} = 0.55$, indicating that some residual non-precipitation echoes at stratiform rain regions have been properly identified. We have verified the same conclusion for the other cases.

b. Dependence of membership functions on different intervals of reflectivity

Fig. 7 shows the skill scores and accumulation with the reflectivity dependent membership functions and a single membership function. In general, reflectivity dependent membership functions significantly increase the skill scores. For example, CSI and ETS increase by about 0.07 at $MF_{thresh} = 0.55$. POD also increases and FAR decreases. These results are due to the mis-classification of precipitation echoes as non-precipitation echoes by the single membership function as can be deduced from Fig. 5 for Z ≥ 30 dBZ. This can be shown in the 5-h rainfall accumulation in Fig. 7c and d. Non-precipitation echoes are effectively removed in both accumulation maps. However, the reduction in rainfall accumulation east of the radar caused by eliminating precipitation echoes of Z ≥ 30 dBZ is noticeable (Fig. 7d) because the total membership value for strong reflectivity is always overestimated. In general, reflectivity dependent membership functions provide the large amount of accumulation at overall regions. These results suggest the importance of proper membership functions as a function of reflectivity.

d. Comparison with the polarimetric approach

The performance of our proposed fuzzy logic method is compared with that of the polarimetric approach in terms of rainfall accumulations.

Rainfall accumulations for three cases are shown in Fig. 8. The first (29-Aug-2004) is a typical convective precipitation with normal ground echoes. Strong AP is present in the other two cases. On 8 July 2004, scattered showers first approach from the south-west and are then followed by stratiform rain mixed with AP. On 19 July 2004 case, strong convective lines and several isolated convective cells approach from the south-east and become weaker after passing by the radar site. Non-precipitation echoes are not removed on the accumulation of the first column. A proposed fuzzy logic and polarimetric methods are applied to eliminate non-precipitation echoes for the second and third columns, respectively.

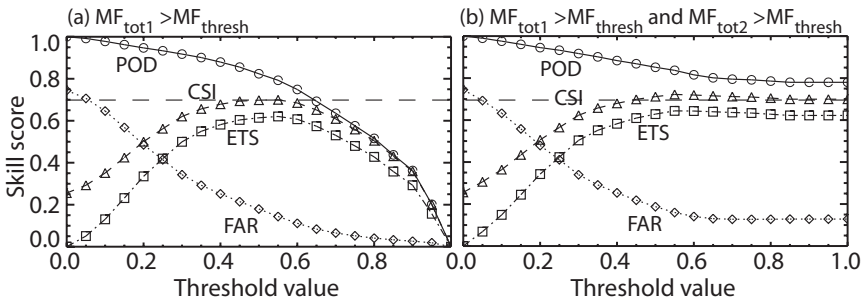

Fig. 6: Skill scores after applying an identification with (a) $MF_{tot1} > MF_{thresh}$ and (b) $MF_{tot2} > MF_{thresh}$ and $MF_{tot1} > MF_{thresh}$

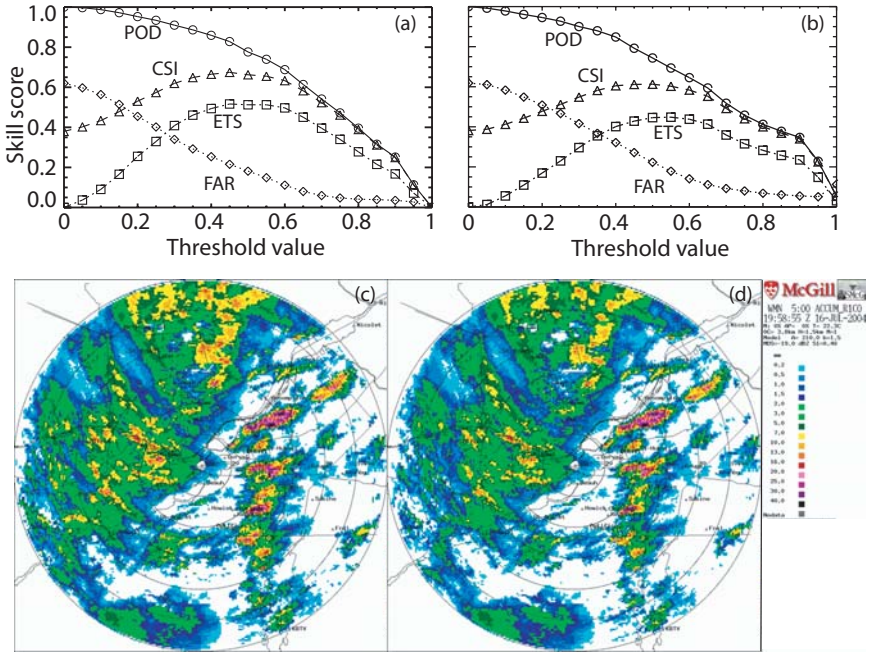

Fig. 7: Skill scores and 5-h rainfall accumulation for the case of 16 July 2004.
(a), (c): from reflectivity dependent membership functions.
(b), (d): single reflectivity independent membership function.

Unrealistically large rainfall amounts are shown in Fig. 8a over the normal ground echo regions, north, south, and south-east of the radar map. In the second and third cases, the accumulation map is further seriously contaminated by AP. The application of the proposed fuzzy logic method removes most of ground echoes and AP without affecting the precipitation echoes. The resultant accumulation map is similar to the one derived with the polarimetric approach. A quantitative analysis has revealed that polarimetric accumulation is slightly larger, indicating that our proposed fuzzy logic method eliminates some of precipitation fields. However, the polarimetric approach could not completely eliminate AP over the indicated area shown in Fig. 8i south of the radar, suggesting that a further optimization of the polarimetric approach is also needed.

6. Conclusion

We have explored the characteristics of precipitation and non-precipitation echoes and have used them in removing non-precipitation echoes. The proposed fuzzy logic method applies reflectivity dependent membership functions and shows thus an improvement over a simple membership function as done by previous researches. The fuzzy membership functions and the proper weights are derived from the distribution of the characteristics of precipitation and non-precipitation radar echoes. In this sense, our approach is more objective and can be easily adapted to local conditions.

Results show that even in Montreal environment, the characteristics of non-precipitation echoes such as the standard deviations of reflectivity, the vertical gradient of reflectivity, and the absolute Doppler radial velocity vary systematically with intensity (radar reflectivity) whereas they are almost constant for the precipitation echoes. Accordingly, the membership functions and weights are made to change with echo intensity unlike what has been done previously by other researchers who have used a single membership function for the entire range of echo intensities. Our evaluation has shown that the use of a single membership function leads to a significant removal of precipitation echoes since, in the heavy

precipitation, the membership value is always overestimated.

The vertical gradient of reflectivity is a key parameter when Z ≥ 30 dBZ and its importance diminishes with decreasing intensity, leading to the Doppler radial velocity as the most effective parameter (Table 1). In general, strong echoes are less ambiguous, resulting into a clear classification. The evaluation shows that the current approach has comparable performance with polarimetric approach. The proposed fuzzy logic method removes most normal ground echoes and AP although some of precipitation fields are eliminated as shown in the comparison of accumulation maps (Fig. 8).

The proposed method is simple and can be applied to any operational radar after deriving the proper membership functions and weights suitable for the local environment.

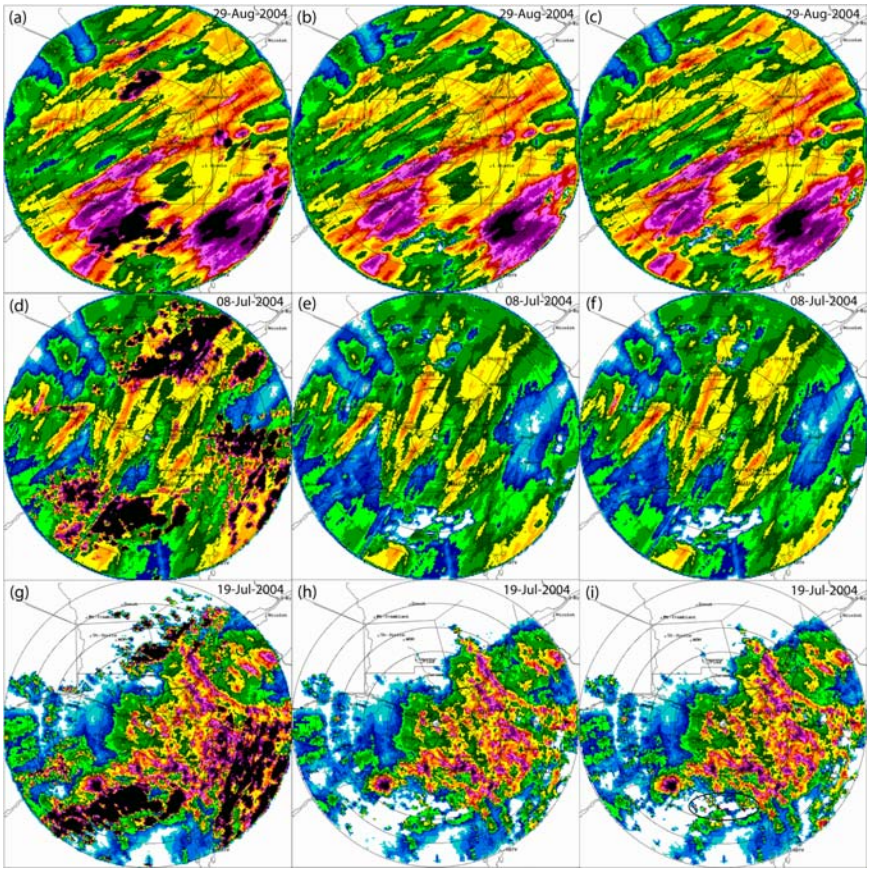

Fig. 8: Rainfall accumulation for three cases (29 Aug. 2004: 4 h accumulation, 08 July 2004: 6 h accumulation, 19 July 2004: 5 h accumulation). Non-precipitation echoes are not removed in the first column. The proposed fuzzy logic and polarimetric methods are applied to each volume scan to remove non-precipitation echoes in the second and third column, respectively.

References

Grecu, M., and W. F. Krajewski, 2000: An efficient methodology for detection of anomalous propagation echoes in radar reflectivity data using neural networks. *J. Atmos. Oceanic Technol.,* **17,** 121–129.

Giuli, D., M. Gherardelli, A. Freni, T. A. Seliga, and K. Aydin, 1991: Rainfall and clutter discrimination by means of dual-linear polarization radar measurements. *J. Atmos.*

Kessinger, C., S. Ellis, and J. VanAndel, 2001: NEXRAD data quality: The AP clutter mitigation scheme. *30th Int. Conf. on Radar Meteorology, Munich, Germany, Amer. Meteor. Soc.,* 707~709.

Lee, G. W. and I. Zawadzki., 2005: Variability of drop size distributions: Time scale dependence of the variability and its effects on rain estimation. *J. Appl. Meteo.*, **44**, 241-255.

Ryzhkov, A. V., and D. S. Zrnic, 1998: Polarimetric rainfall estimation in the presence of anomalous propagation. *J. Atmos. Oceanic Technol.,* 15, 1320~1330

Steiner, M. and J. A. Smith, 2002: Use of three-dimensional reflectivity structure for automated detection and removal of nonprecipitating echoes in radar data. *J. Atmos. Oceanic Technol.,* 19, 673-686.

Steiner, M., J. A. Smith, C., Kessinger, and B. S. Ferrier, 1999: Evaluation of algorithm parameters for radar data quality control. Preprints, 29th Int. Conf. on Radar Meteorology, Montreal, QC, Canada, Amer. Meteor. Soc., 582–585.